Chirality Switching in Ferromagnetic Nanostructures Via Nanosecond Electric Pulses

W. A. S. Aldulaimi, C. Akaoglu, K. Sendur, M. B. Okatan, and I. B. Misirlioglu*

The stability of magnetism in reduced dimensions has become a major scientific agenda in the pursuit of implementing magnetic nanostructures as functional components in spintronic devices. Methods to probe and control magnetization states of such structures in a deterministic manner include use of spin polarized currents, photon absorption, and relatively recently, electric fields that tailor magnetoelectric coupling in multiferroic based structures. In theory, a short electric pulse is able to generate localized magnetic fields that can couple to the local magnetic dipoles electrodynamically. Here, using the Landau–Lifshitz–Gilbert formalism of magnetism dynamics combined with continuum Maxwell relations, the response of a ferromagnetic permalloy nanodisc to nanosecond electric field pulses is studied. The dynamics of the magnetic order of the nanodiscs during this process are examined and discussed. Ferromagnet nanodiscs, when below a critical size and in the absence of any external field, relax to a vortex phase as the ground state due to the demagnetizing field. Simulations demonstrate that the planar chirality of such a ferromagnet nanodisc can be switched via a time-wise asymmetric electric field pulse on the order of a few ns duration that generates radially varying tangential magnetic fields. These fields couple to the vortex state of the nanodisc ferromagnet electrodynamically, revealing an effective and robust method to control chirality.

1. Introduction

Ferromagnetism has a very unique role in the computer revolution since a significant portion of the data storage technology relies on this property that several metals and alloys intrinsically exhibit. Driven by the downscaling of integrated circuits

(ICs), ferromagnetism in reduced dimensions has become a field of research. Recently, a renewed interest has been devoted to study ferromagnets in reduced dimensions due to the reporting of some exotic phases and orderings absent in bulk. Nanodiscs are among such class of systems and were shown to attain magnetic vortex-type order when below a critical radius where the system size becomes comparable to domain wall widths.[1,2] Vortex ordering in the magnetic state has unique properties such as a minimum stray field, faint interaction between the adjacent nanodiscs when in the form of arrays, and high thermal stability against fluctuations.[3–8] These characteristic features make the ferromagnet nanodiscs appealing for spintronic applications, such as high density magnetic data storage, logic devices,[2,8–11] and in microwave oscillators.[12,13] Vortex states are of interest in particular as the clockwise (CW) or counter clockwise (CCW) states could allow a memory function in an extremely small volume.

Despite the attractive potential of tailoring vortex states in nano magnets, a limited number of works have focused on chirality switching of these structures both experimentally and computationally.[14–18] One forthcoming major challenge is to achieve swift and repeatable control of magnetism in these structures and establish chirality switching in a time period desirably not exceeding a few nanoseconds. Generally, the vortex state is not a stable state in bulk: Order stability maps have been generated where chiral ferromagnetic states were shown to depend on the aspect ratios and geometry.[19–23] In refs. [18–22], the phase stabilities of various ferromagnetic states in phase diagrams of nanostructures reveal that a unit must have a distinct aspect ratio to obtain a magnetic vortex state. If there is no shape anisotropy, the CW and CCW states are degenerate and they may emerge randomly as equilibrium states.[7,24] A number of works have focused on shape-wise anisotropic micromagnetic systems: Such constructs require precise adjustments or the sought magnetic vortex configuration cannot be stabilized.[24–28] In addition to planar chirality, a magnetic vortex possesses another parameter known as polarity which describes the magnetization direction at the vortex center and various methods were proposed to manipulate the polarity such as bursts of magnetic fields, spin-polarized currents and optical manipulation.[10–12,29–31] Luo

W. A. S. Aldulaimi, K. Sendur, I. B. Misirlioglu
Faculty of Engineering and Natural Sciences
Sabanci University
Orhanli/Tuzla, Istanbul 34956, Turkey
E-mail: burc@sabanciuniv.edu
C. Akaoglu
Department of Materials
University of Manchester
Manchester M13 9PL, United Kingdom
M. B. Okatan
Department of Materials Science and Engineering
Izmir Institute of Technology
Gulbahce/Urla, Izmir 35430, Turkey

The ORCID identification number(s) for the author(s) of this article can be found under https://doi.org/10.1002/andp.202100167
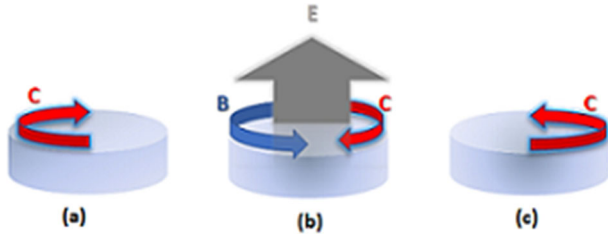
Figure 1. a) Schematic of a magnetic vortex state with a CW chirality, C, (red arrow) in a nanodisc. b) Application of a time-wise asymmetric electric field, E, (gray arrow) which induce a radially varying tangential magnetic field, B, (blue arrow). c) The chirality switches from CW to CCW upon the pulse generated field reaching a critical amplitude within a critical duration.

et al. have reported polarity switching to occur simultaneously below a critical disc size whereby the method they used to simulate switching was passing a direct current along the disc normal driving an Oersted field.[18] Experimentally, due to the spatial variation of magnetic order, investigation of the polarity switching dynamics possesses challenges and is pursued in a limited number of attempts.[7]

In a circular ferromagnetic disc, it is difficult to control the vortex chirality by applying an in-plane, homogeneous magnetic field,[24] which is often the concept GMR and TMR based device designs are centered around. Several micromagnetic simulation studies have reported outputs on how a magnetic vortex can react to an externally applied field.[12,26,32–35] One drawback of a direct magnetic induction based control is that it is almost impossible to confine a magnetic field to a small volume when the structure of interest is in reduced dimensions.[36] The vortex state could also be switched under an inhomogeneous magnetic field generated by electrical currents passing through a wire along the plane normal. Here, the inhomogeneity is generated by using a mask to shield part of the disk from the field effect. However, the acquisition of the localized pulse obtained is often not feasible to utilize in an application.[37] An inhomogeneous field drives gradients of magnetism away which favors the stabilization of a uniform order of magnetism. This is difficult to utilize in practice. Surface probing methods can effectively "write" magnetic patterns via a magnetic tip,[33] but cannot go beyond the laboratory scale.

In this work, we propose tailoring time-wise asymmetric electrical pulse signals on the order of ns durations to control the chirality of vortex states in ferromagnetic nanodiscs. Using the LLG formalism coupled with Maxwell relations, we demonstrate that such pulses can generate radially varying tangential magnetic fields (these fields will be called "tangential fields" from here onward) coupling electrodynamically to the magnetic dipoles, capable of switching the chirality of the ferromagnet nanodiscs for which the vortex phase is the ground state. This idea is depicted schematically in **Figure 1**. As for the material, we consider permalloy $Ni_{80}Fe_{20}$, a composition with well identified phenomenological parameters. We demonstrate that chirality of this system can be switched upon application of a time-wise asymmetric electric pulse signal via a voltage drop between the two surfaces of the disc along the z-axis, generating a tangential magnetic field whose amplitude reaches a maximum at the disc edge. This article is organized as follows: The theory and simulation

details are provided in Section 2, the magnetization dynamics of the vortex chirality reversal process, including the time evolution of the asymmetric electric field pulse are given in Section 3, followed by conclusions in Section 4.

2. Theory and Simulation

In this section, we give the governing equations for the micromagnetic simulations, which are performed utilizing a finite-difference scheme. The generic LLG equation governing magnetization dynamics is written as[38]:

$$
\frac{d\mathbf{M}}{dt} = -\frac{\gamma}{1+\alpha^2}(\mathbf{M} \times \mu_o \mathbf{H}_{\text{eff}})
$$
$$
-\frac{\alpha\gamma}{(1+\alpha^2)M_s}[\mathbf{M} \times (\mathbf{M} \times \mu_o \mathbf{H}_{\text{eff}})]
$$

(1)

where $\mathbf{M}$ is a magnetization vector $\mathbf{M} = (\mathbf{M}_x, \mathbf{M}_y, \mathbf{M}_z)$, α is the damping constant, γ is the gyromagnetic ratio, M_S is the saturation magnetization, and $\mathbf{H}_{\text{eff}}$ is the effective magnetic field. The first term is the precession of magnetization which arises due to the interaction between local spin with $\mathbf{H}_{\text{eff}}$. The second term provides a damping of the precessional motion which aligns the magnetization along the $\mathbf{H}_{\text{eff}}$ direction. $\mathbf{H}_{\text{eff}}$ includes the external and the internal fields derived from the magnetic energy density, $\mathbf{E}$, i.e, $\mathbf{H}_{\text{eff}} = -\frac{\partial \mathbf{E}}{\mu_o \partial \mathbf{M}}$:

$$
\mathbf{H}_{\text{eff}} = \mathbf{H}_{\text{exch}} + \mathbf{H}_{\text{anis}} + \mathbf{H}_{\text{demag}} + \mathbf{H}_{\text{ext}}
$$

(2)

$\mathbf{H}_{\text{exch}}$, $\mathbf{H}_{\text{anis}}$, $\mathbf{H}_{\text{demag}}$, and $\mathbf{H}_{\text{ext}}$ are the exchange field, anisotropy field, demagnetization field, and external field, respectively.[39] On the boundaries of the system, we employed the Neumann boundary conditions as the following:

$$
\frac{\partial \mathbf{M}_n}{\partial \mathbf{n}} = 0
$$

(3)

where $\mathbf{n}$ is the normal to the boundary of the nanodisc.

In our simulations, the system is supposed as surrounded by vacuum, which requires the solution of the magnetic fields outside of the system too, unlike similar works. This is one of the factors that drive vortex formation given that the system size is far too small to form distinct domains to minimize the demagnetizing fields arising from the system boundaries. The simulations are performed on a 95 nm diameter permalloy nanodisc whose typical material parameters are the saturation magnetization $M_s = 8 \times 10^5$ A/m, the exchange constant $A = 1.3 \times 10^{-11}$ J/m, the exchange length $\lambda_{ex} = 5.29$ nm, and we choose a Gilbert damping parameter $\alpha = 0.02$.[34,40] The thickness of the disc is 11.4 nm. For such aspect ratios (radius and thickness to exchange length), the simulated structures fall into the vortex stability regime as previously reported in refs [19–22]. The cell size is $1.9 \times 1.9 \times 1.9$ nm^3 in all the simulations. The total time for the simulations is 3 ns, consisting of 5 fs steps corresponding to 600 K iterations. The initial equilibration of the discs before any applied pulse was done with 400 K iterations starting from a random distribution of directions for the magnetic moment components $\mathbf{M}_x$, $\mathbf{M}_y$, and $\mathbf{M}_z$ as the initial state whereby each

**ADVANCED
SCIENCE NEWS**

www.advancedsciencenews.com
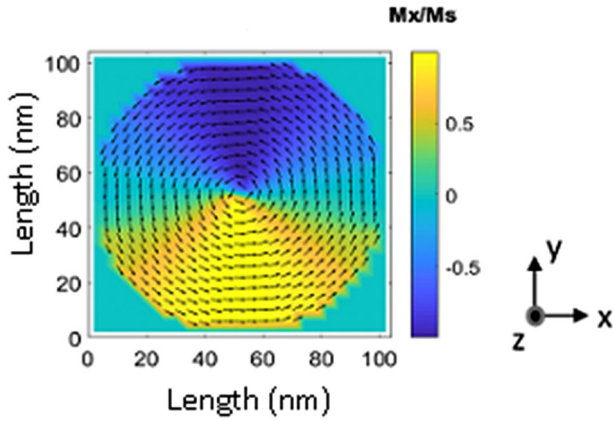
annalen
der **physik**

www.ann-phys.org

Figure 2. Planar magnetization vector map of the permalloy 95 nm diameter nanodisc in its ground state attain the vortex configuration. The colormap superimposed on the vectorial plot here shows the Mx component for convenience. Upon switching, the upper and lower shades switch, indicating chirality switching.

local moment satisfies the amplitude $\sqrt{(\mathbf{M}_x^2 + \mathbf{M}_y^2 + \mathbf{M}_z^2)} = M_s$. The ground state of the nanodisc after 400 K iterations that has evolved under zero field is given in **Figure 2**. The magnetocrystalline anisotropy in permalloy depends on the stoichiometry of Fe and Ni, and the composition that we use in our calculation has the formula $Ni_{80}Fe_{20}$ possessing zero values for K_1 and K_2, which are the anisotropy constants as reported in refs [41–43].

Before going onto the effect of an electric pulse on a magnetic structure, it is useful to revisit the classical relations in electrodynamics for convenience. Electrically induced magnetic fields in a nanodisc setting can be generated in two ways: either by direct electric current through the disc or via time varying electric fields. The fundamental relation connecting the magnetic field, **B** along the closed boundary of an area through which a current density **J** or a dielectric flux **D** passes is:

$$\oint \mathbf{B}.d\mathbf{l} = \mu_o \left(\int \mathbf{J}.\mathbf{ds} + \frac{d}{dt} \int \mathbf{D}.\mathbf{ds} \right) \tag{4}$$

μ_o is the permeability of free space, $\mathbf{D} = \epsilon_o \mathbf{E}$, ϵ_o is the permittivity of free space. **E** points along the normal of the disc (z-axis). Considering the skin depth and dielectric relaxation time of permalloy, we assume that no electric current is passing through the disc resulting in $\mathbf{J} = \mathbf{0}$; therefore, the first term on the rhs is neglected, leaving us with the time-dependent relation:

$$\oint \mathbf{B}.d\mathbf{l} = \mu_o \left(\frac{d}{dt} \int \mathbf{D}.\mathbf{ds} \right) \tag{5}$$

From this equation, it is easy to deduce the relation between the magnetic induction **B** and electric field **E** is:

$$2\pi r B(r) = \mu_o \epsilon_o \pi a^2 \frac{dE}{dt} \tag{6}$$

with a being the disc radius and r is the radial coordinate at which we measure **B**. To be able to induce a one-way switching, one needs to design an electric pulse that is asymmetric in time.

Asymmetric half-cycle-pulses are generally feasible, and widely used both experimentally and theoretically. The following equation can be chosen to describe such a pulse shape[44]:

$$E(t) = E_0 \frac{t}{\tau_o} \left[\exp\left(-\frac{t^2}{2\tau_o^2}\right) - \frac{1}{b^2} \exp\left(-\frac{t}{b\tau_o}\right) \right] \tag{7}$$

where $E(t)$ is a function of time, and τ_o and b are parameters to determine the duration and the asymmetry of the pulse, respectively. We designed such a pulse as given in **Figure 3**a with various durations. E_0 is 0.09 V/nm, b is 180 for all pulses, and τ_o is 0.25, 0.35, 0.45, and 0.65 ns for the black, red, blue, and green pulse, respectively. A pulse in accordance with Equation (7) has a steep positive slope (head) and a negative slope (tail) asymmetrical in time, that is vital if a one-way switching of the chirality is desired. If the pulse is along +z-axis, then the initial positive slope region of the pulse generates a CW traversal magnetic field while the negative slope region generates CCW traversal magnetic field. We utilize the negative slope region of the pulse to induce vortex chirality reversal. We note that the use of an asymmetrical pulse to induce chirality switching was mentioned in ref. [34] but not checked. The magnetic field strength along the periphery of the nanodiscs ($B(r)$) varying over time as a result of the electric flux of the pulse is presented in Figure 3b. It is the radial magnetic field whose maximal value is plotted in Figure 3b that enters the simulations as $\mathbf{H}_{ext}$ in Equation (2).

3. Results and Discussion

The ground state vector map of the disc considered for this work is provided in Figure 2 displaying the vortex phase as the stable state with a CCW orientation obtained beyond 400 K iterations after which we noted that the system does not evolve further. This solution constitutes the initial condition for when an electric signal is to be applied to induce switching of the chirality. The chirality of the nanodiscs were tracked under the pulse shown in Figure 3a with the accompanying edge magnetic fields (Figure 3b) in Figure 3c. We note that there exists a critical pulse duration for chirality to reverse or else switching does not proceed (see the green data in Figure 3a for the pulse and 3(c) for chirality). The amplitude of the tangential magnetic field to induce switching of chirality depends on the time derivative of the electrical pulse signal as seen in Equation (6): $d(E)/dt < 0$ yields a CCW and $d(E)/dt > 0$ yields a CW radial magnetic field. Keeping this in mind, the two electrical pulse signals (red and black) shown in Figure 3a, can switch the vortex state in about 1.5 ns after which the system remains stable in the CW state, and thus a reversed chirality state is obtained. However, under the (blue) pulse, the system requires more time to relax into the CW state. As expected from Equation (6), a longer electrical pulse signal generates a weaker magnetic field owing to the shallower slope in relation to the time axis. To overcome this, the strength of the electric pulse needs to be increased or otherwise chirality switching does not occur. We find that the electrical pulse signals required to induce switching can be shorter than 1 ns if the electrical signal strength is higher than 0.55 MV/cm.

Figure 4 shows temporal evolution of the chirality from CCW to CW state after applying an electrical pulse signal of a strength

**ADVANCED
SCIENCE NEWS**

www.advancedsciencenews.com

annalen
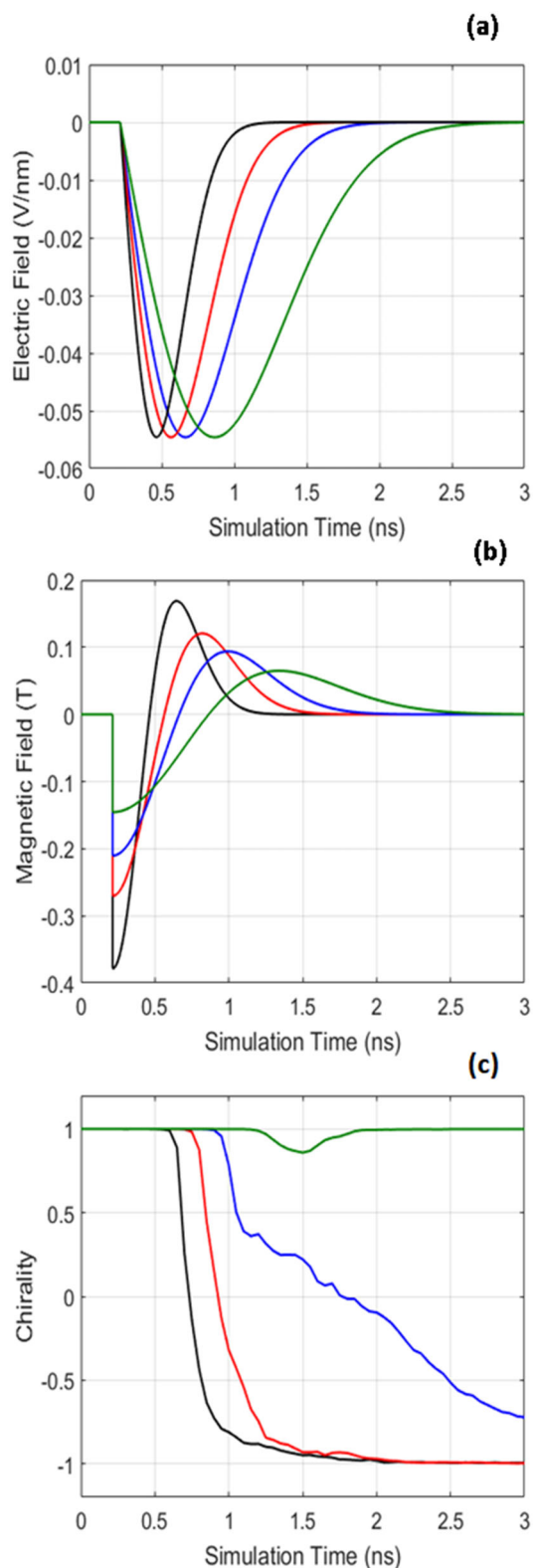der **physik**

www.ann-phys.org

Figure 3. a) The time-varying ns electrical pulses with different widths constructed from Equation (7). b) The accompanying peripheral value of the (max. of B_{ext}) magnetic fields derived from Equation (6). c) The overall average chirality response of the ferromagnetic disc under the action of the electric pulse signal given in (a).

approximately 0.55 MV/cm along z-axis. Note that at $t = 0$, the system is in its ground state whose data is given in Figure 2. For an applied electric field pulse (black signal Figure 4a), the switching starts with loss of order of the magnetic moments that are near the edge where the radially generated magnetic field is maximum as shown in Figure 4(c-2). As the boundary sites lack neighbors, the electric pulse induced magnetic field at its maximum value dominates over the exchange field, realigning these magnetic moments. However, the initial CCW vortex core (yellow dot) (See Figure 5(3)) still remains and spatially oscillates near the center at the time when the signal is turned off. Note that at 1 ns, a new vortex CW core (blue dot) starts to nucleate, with time evolution the CW and CCW cores start to interact (Figure 5(3–7)), and a yin-yang type of transient state near the center is observed where the magnetization aligns with the field under a Zeeman torque near the edges where the magnetic induction is at its highest. Eventually, CCW yellow core is annihilated which is observed between (1.9–2.1) ns, leaving its position to the CW (indicated by the blue core in Figure 5(7–8)). Apart from $\mathbf{H}_{ext}$ being maximal at the disc periphery, that magnetization vectors near the edge of the nanodisc experience a higher demagnetizing field make these dipoles respond earlier to the pulse-induced magnetic field compared to the interior sites of the disc. Similarly, in exactly the same manner, the vortex can be switched back into the CCW configuration with an electrical pulse signal in the +z direction. Thus, a deterministic and swift switching of the chirality is possible to achieve with the primary coupling of the $\mathbf{B}$ to $\mathbf{M}$.

In order to be able to track layer-wise variations associated with the vortex core, first its coordinates in the plane of the disc need to be determined in each layer of the disc, that is, through the thickness of the disc. For this purpose, at each magnetic dipole site, ij in a given layer, we calculated the chirality "both spatially and globally" given by:

$$Chirality = \frac{1}{nM_s} \oint \mathbf{M}.d\mathbf{s} \tag{8}$$

where M is the magnetization in the XY-plane of the disc and ds is the arc length of the path which was chosen as the circle centered at the magnetic dipole site with a radius equal to the dipole-dipole separation on the computational grid. In Equation (8), n is the number of sites over which the integral is evaluated. M values on a given path were determined via bilinear interpolation, a method used to form continuous curves on discrete set of data points, especially when one has to evaluate an analytical expression such as in the case of chirality defined as an integral over a closed continuous path. For the spatial chirality mapping procedure, magnetization components of the nearest and next nearest sites neighboring a given coordinate i,j were used. In order to track the global chirality of the disc, this procedure was applied to concentric circular paths with the disc center being the reference coordinate whose average chirality yielded results such as in Figure 4b. Chirality attains values ranging between -1 and +1 for CW and CCW oriented vortices, respectively, and a value of zero for a homogeneously magnetized media. Under the action of the black pulse shown in Figure 3a, we use Equation (8) as prescribed to track the vortex core position(s) and locate its coordinates on the vector field map of the magnetic dipole moments (MDMs), as shown in Figure 5. The magnetic vortex cores
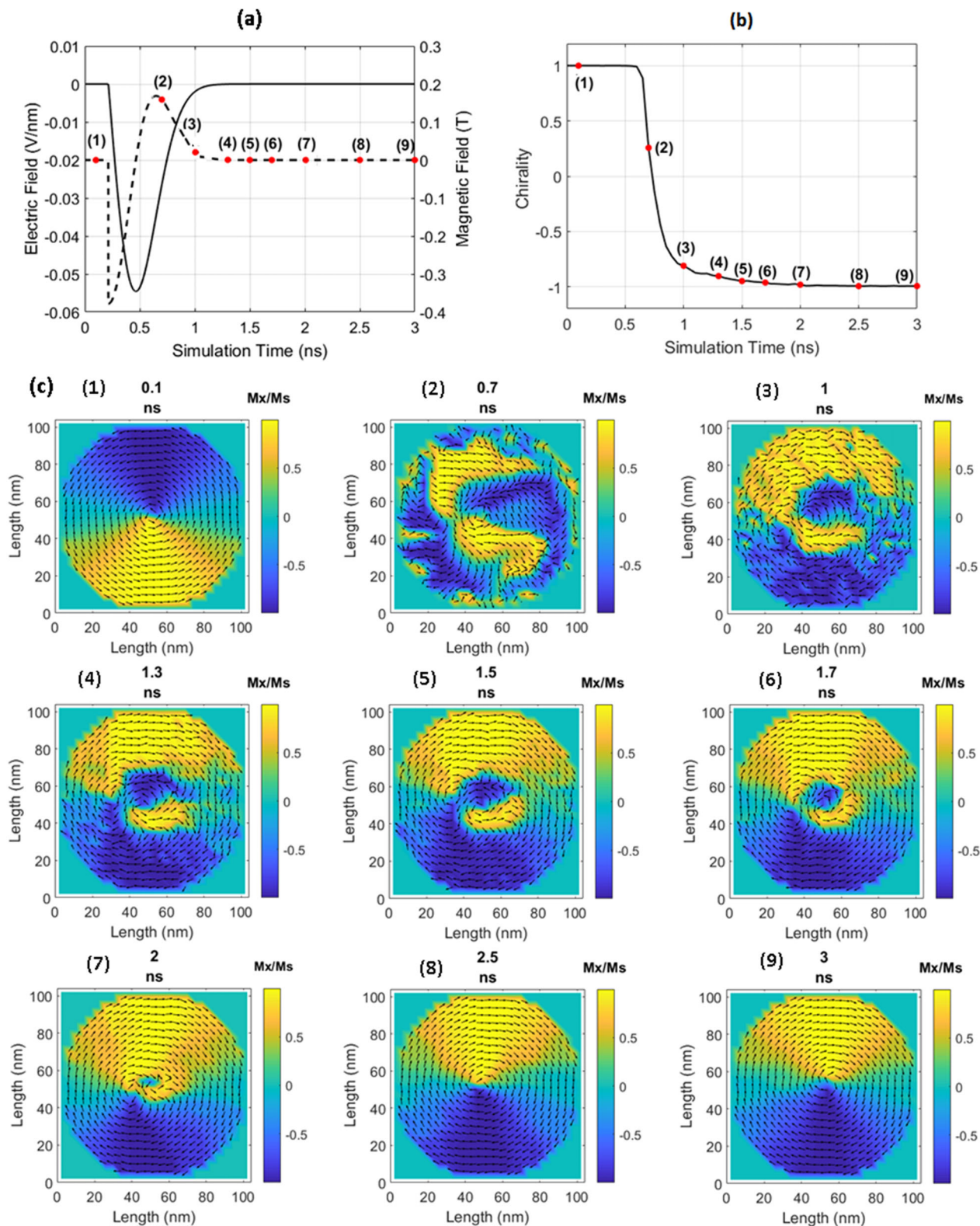
Figure 4. a) The time-varying ns electrical pulse and the accompanying magnetic field derived from Equation (6) where the solid line is the electric field and the dashed line is the accompanying radial magnetic field. b) Chirality of the system in response to the pulse given in (a). Red points labeled as (1–9) in (a) are the instants where we show the planar magnetic dipole configurations in (c) in response to the time varying electric pulse. The vortex states in (1) and (9) are anticlockwise and clockwise, respectively, indicating that switching has occurred. Vortex switching starts between (2) and (6) when $B > 0$ accompanied by an oscillation in the vortex center position (See **Figure 5**).
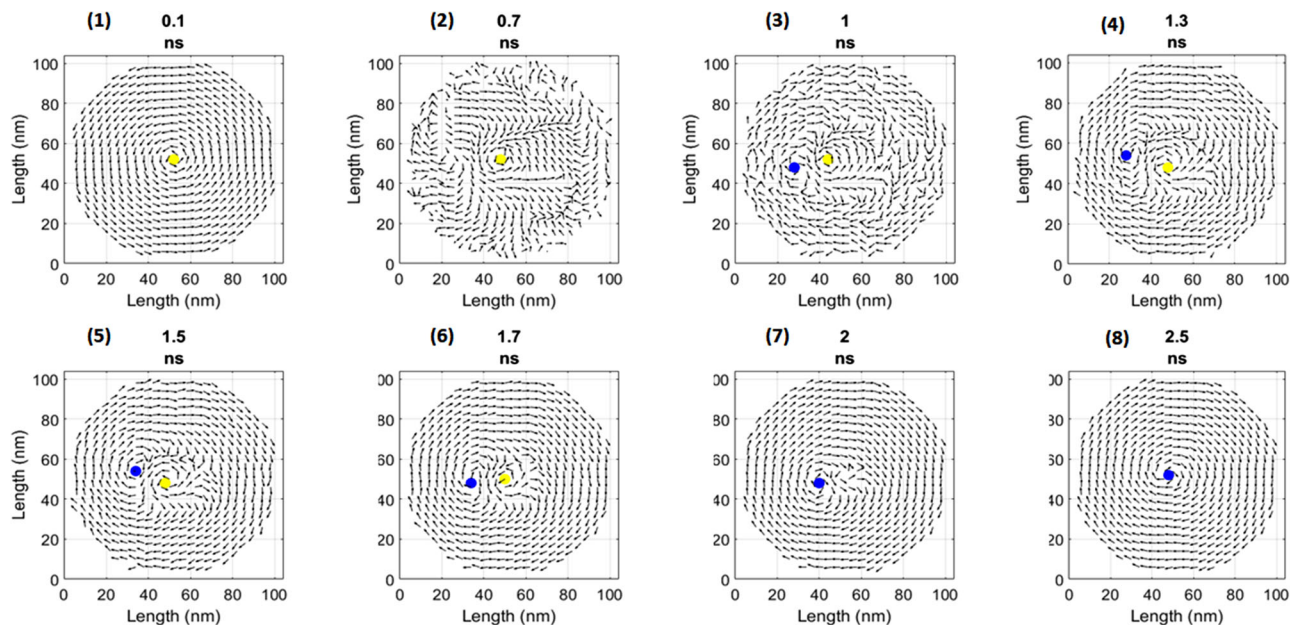
Figure 5. The temporal evolution of the vortex core position during the simulations under the (black pulse given in Figure 3a) given along with the in-plane magnetization vector variation. The yellow dot belongs to the CCW state and the blue dot representing the formation of a local CW order appears during the switching process under field, eventually replacing the yellow dot as seen in (7) and (8).
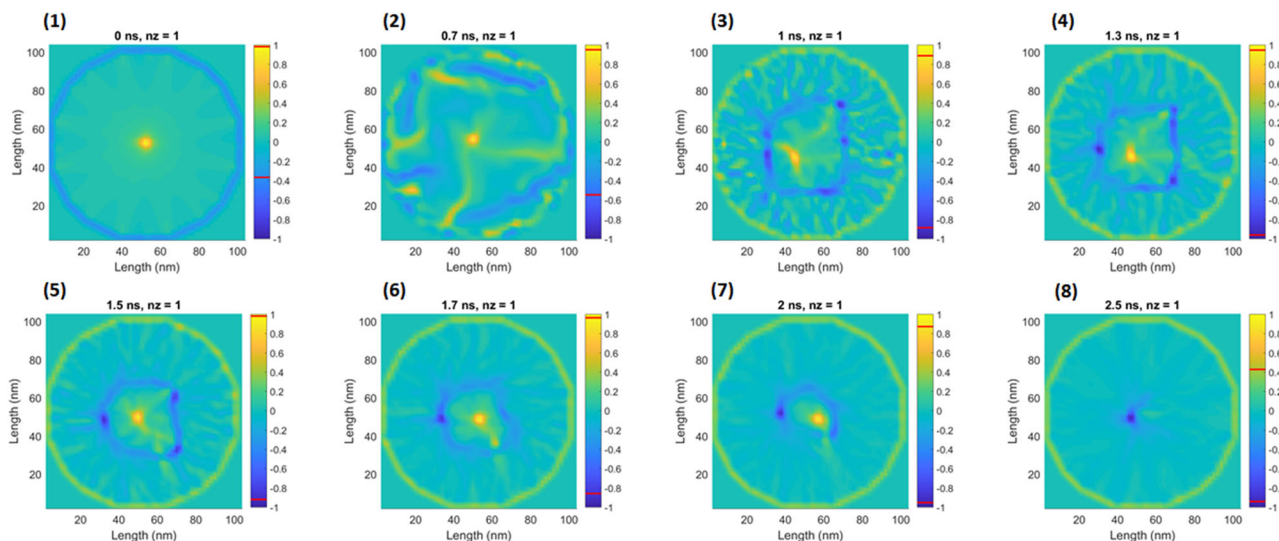

Figure 6. The temporal evolution of the vortex chirality from CCW ($c = 1$) with vortex core (yellow dot) to CW ($c = -1$) with vortex core (dark blue dot).

($|Chirality| > 0.8$) are labeled as a yellow dot for the CCW vortex orientation while a blue dot for CW vortex orientation. During switching, two cores can appear: At 1 ns, a new vortex core starts to nucleate with CW orientation near the center. Although the signal is turned off (see Figure 3a at 1 ns), the old CCW remains and oscillates near the center of the disc. As the iterative steps of the simulation progresses, these cores interact while the magnetic dipoles near the disc edge have already switched to the CW state. To keep the demagnetization energy of the system in a local minimum, the MDMs along the periphery tend to be parallel to the disc edge. The exchange interaction for ferromagnetic materials favors the parallel alignment of the neighboring MDMs.

Thus, a configuration according with a CW orientation gradually settles in a dominant portion of the disc after the field is switched off and the CCW core is annihilated at 2 ns as displayed in (7) of **Figure 6.** Eventually, a reversed vortex chirality is stabilized.

Figure 6 presents the color maps which were obtained from Equation (8) where we can visualize the "degree of chirality." The yellow region represents the CCW state while the dark blue region represents the CW state. After applying the electrical signal pulse, a distinct ring forms at approximately 1 ns. This blue "chirality ring" that shrinks in radius with progressing simulation time mainly consists of antiparallel aligned dipole couples along x- and along y- at neighboring sites, yielding an overall

**ADVANCED
SCIENCE NEWS**

www.advancedsciencenews.com
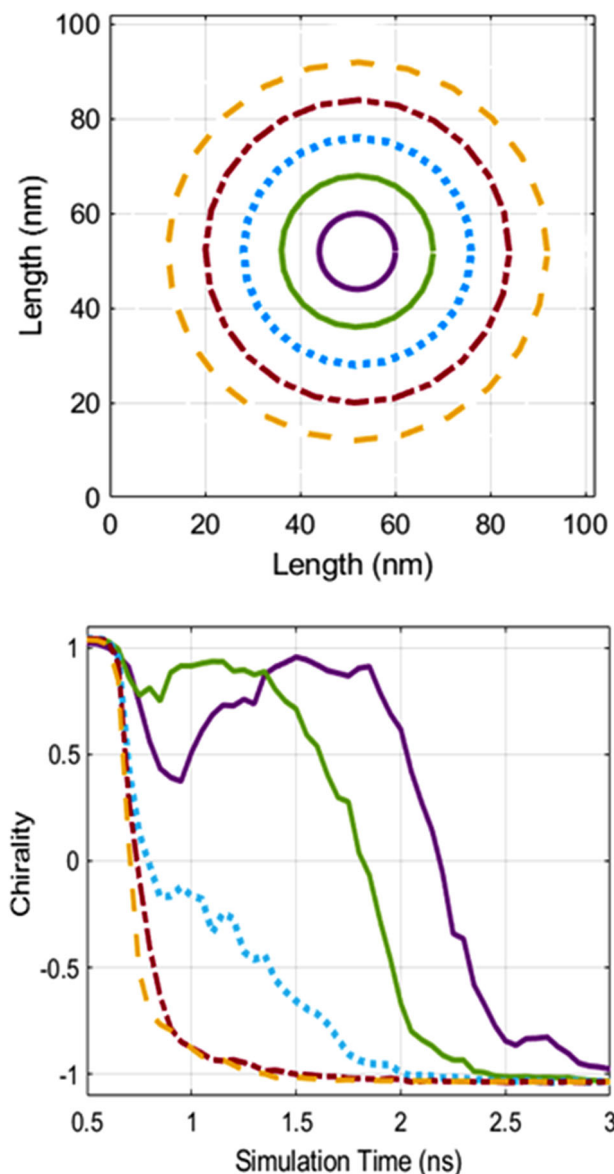
annalen
der **physik**

www.ann-phys.org

Figure 7. a) The circular paths at which we evaluate the average line integral (see Equation (8)). b) The corresponding chirality value for each circular path shown in (a) as a function of time.

negative value chirality locally. Along the ring, nucleation of CW vortices are visible as dark blue spots. These blue rings separate "switched" regions close to the disc periphery than regions that are "about to switch", which we deduce from the plot in **Figure 7**. Here, we provide the average of the line integrals along circles at various distances to the center (See Equation (8)). It can be seen that along the paths close to the disc periphery, switching has occurred as can be deduced from the change of the average line integral value for these circular paths. The same value for the inner rings fluctuate between 1 and 0.5 until around 1.5 ns, implying gradual disappearance of the CCW order representing these regions followed by changing of chirality sign after around 1.75 ns. The blue rings corresponding to negative chirality appear inside of the nanodisc at around 0.7 ns and denote the boundary

between the two tendencies. They gradually merge into a single ring, which acts as a site for nucleation of an at least one CW vortex that annihilates the CCW vortex at the center belonging to the state preceding the application of the electric pulse. The latter remains almost all the way through the switching process. We also note the manner with which the blue rings form near the periphery, first as individual segments that later on coalesce and shrink toward the center related to the radial dependence of the magnetic field induced by the electric pulse. The very same reason causes an inhomogenous switching that start from the edges where the pulse induced magnetic field is at its max. We deduce so because a virtual circular but homogeneous magnetic field does not induce such formations during switching (not shown here). It is the maximal value of the magnetic field at the periphery of the disc induced by the electric flux that causes the CW alignment parallel to the planar magnetic field direction. With further steps in the simulation, this ring gets smaller in diameter, rendering more dipoles switching toward the CW state emanating from the switching of dipoles propagating toward the interior. A dark blue region (CW nucleation) starts to appear (on the left side of the yellow region), and between 2 and 2.2 ns timesteps, the yellow region that was the core of the CCW state disappears, and the dark shade representing the vortex with CW chirality locates itself in the center, stabilizing the global CW state. Please note that the apparent non-zero chirality at the disc periphery at all times is due to the fact that sites along this periphery lack neighbors and yield a non-zero result for the integration of Equation (8) and is therefore an artificial effect, although it is sensitive to the magnetization direction.

4. Conclusion

We have demonstrated, using the LLG formalism, that a timewise asymmetric electric pulse with a critical amplitude and duration can be designed to induce chirality switching via electrodynamic coupling to the magnetic dipoles in the nanodisc within ns timescale. We tracked the degree of chirality in the nanodisc structure that allowed us to characterize the switching process. The chirality switching process occurs in three steps: First, the magnetization near the disc edge loses the order and switches into the opposite direction after coupling to the tangential magnetic field where the field amplitude is at its maximum. In parallel, a "chirality" ring appears to be nucleating from which a distinct new center forms that is attracted to the central "old" core. Finally, the old core disappears and the new one locates itself in the center. We also note that, during chirality switching, the polarity of the magnetic vortex can vary several times and therefore the deterministic control of the polarity state appears to be difficult to control. In the case of an array of discs with some radial size distribution to perform a specific action such as memory storage, the needed pulse duration and amplitude depends on the area enclosing the electric flux intersecting the disc along the disc normal. Therefore, the dependency of the azimuthally induced magnetic field as a result of the time derivative of the electric flux needed to switch the chirality of a nanodisc could vary slightly. In addition, in connection with the size dependence of the ferromagnetic phase stability in such systems, smaller fluxes of an electric pulse might suffice to induce switching compared to discs with larger radii. In summary, we were able to demonstrate

electric pulse switching of chirality of a ferromagnetic order stabilizing in the vortex state. Our current findings for the dynamic magnetic vortex switching via electric pulses are of direct and significant relevance for applications such as data storage in reduce dimensions and magnetic logic devices relying on magnetoresistive effects.

Conflict of Interest

The authors declare no conflict of interest.

Data Availability Statement

Data sharing is not applicable to this article as no new data were created or analyzed in this study.

[1] J. Tóbik, V. Cambel, G. Karapetrov, *Phys. Rev. B* **2012**, *86*, 134433.
[2] T. Shinjo, T. Okuno, R. Hassdorf, K. Shigeto, T. Ono, *Science* **2000**, *289*, 930.
[3] H. B. Braun, *Adv. Phys.* **2012**, *61*, 1.
[4] S. D. Bader, *Rev. Mod. Phys.* **2006**, *78*, 1.
[5] R. P. Cowburn, *Nat. Mater.* **2007**, *6*, 255.
[6] S. Sugimoto, Y. Fukuma, S. Kasai, T. Kimura, A. Barman, Y. Otani, *Phys. Rev. Lett.* **2011**, *106*, 197203.
[7] X. Fu, S. D. Pollard, B. Chen, B. K. Yoo, H. Yang, Y. Zhu, *Sci. Adv.* **2018**, *4*, eaat3077.
[8] B. Pigeau, G. de Loubens, O. Klein, A. Riegler, F. Lochner, G. Schmidt, L. W. Molenkamp, V. S. Tiberkevich, A. N. Slavin, *Appl. Phys. Lett.* **2010**, *96*, 132506.
[9] K. Bussmann, G. A. Prinz, S. F. Cheng, D. Wang, *Appl. Phys. Lett.* **1999**, *75*, 2476.
[10] B. Van Waeyenberge, A. Puzic, H. Stoll, K. Chou, T. Tyliszczak, R. Hertel, M. Fähnle, H. Brückl, K. Rott, G. Reiss, Neudecker, D. Weiss, C. H. Back, G. Schutz, *Nature* **2006**, *444*, 461.
[11] G. De Loubens, A. Riegler, B. Pigeau, F. Lochner, F. Boust, K. Y. Guslienko, H. Hurdequint, L. Molenkamp, G. Schmidt, A. N. Slavin, V. S. Tiberkevich, N. Vukadinovic, O. Klein, *Phys. Rev. Lett.* **2009**, *102*, 177602.
[12] V. Pribiag, I. Krivorotov, G. Fuchs, P. Braganca, O. Ozatay, J. Sankey, D. Ralph, R. Buhrman, *Nat. Phys.* **2007**, *3*, 498.
[13] A. Khvalkovskiy, J. Grollier, A. Dussaux, K. A. Zvezdin, V. Cros, *Phys. Rev. B* **2009**, *80*, 140401.
[14] R. Antos, Y. Otani, *Phys. Rev. B* **2009**, *80*, 140404.
[15] R. K. Dumas, D. A. Gilbert, K. Eibagi, K. Liu, *Phys. Rev. B* **2011**, *83*, 060415.
[16] V. Uhlíř, M. Urbánek, L. Hladík, J. Spousta, M. Y. Im, P. Fischer, N. Eibagi, J. J. Kan, E. E. Fullerton, T. Šikola, *Nat. Nanotechnol.* **2013**, *8*, 341.
[17] B. C. Choi, J. Rudge, E. Girgis, J. Kolthammer, Y. K. Hong, A. Lyle, *Appl. Phys. Lett.* **2007**, *91*, 022501.
[18] Y. Luo, Y. Wu, C. Yu, H. Li, J. Wen, L. Zhu, Z. Qian, T. Zhou, *Phys. Rev. Appl.* **2019**, *11*, 044090.
[19] K. L. Metlov, Y. Lee, *Appl. Phys. Lett.* **2008**, *92*, 112506.
[20] W. Scholz, K. Y. Guslienko, V. Novosad, D. Suess, T. Schrefl, R. Chantrell, J. Fidler, *J. Magn. Magn. Mater.* **2003**, *266*, 155.
[21] C. Ross, M. Hwang, M. Shima, J. Cheng, M. Farhoud, T. Savas, H. I. Smith, W. Schwarzacher, F. Ross, M. Redjdal, F. B. Humphrey, *Phys. Rev. B* **2002**, *65*, 144417.
[22] R. P. Cowburn, D. Koltsov, A. Adeyeye, M. Welland, D. Tricker, *Phys. Rev. Lett.* **1999**, *83*, 1042.
[23] K. L. Metlov, *J. Appl. Phys.* **2013**, *113*, 223905.
[24] S. Yakata, M. Miyata, S. Nonoguchi, H. Wada, T. Kimura, *Appl. Phys. Lett.* **2010**, *97*, 222503.
[25] N. Vargas, S. Allende, B. Leighton, J. Escrig, J. Mejía-López, D. Altbir, I. K. Schuller, *J. Appl. Phys.* **2011**, *109*, 073907.
[26] Y. Wen, Z. Feng, B. Miao, R. Cao, L. Sun, B. You, D. Wu, W. Zhang, Z. Jiang, R. Cheng, H. Ding, *J. Magn. Magn. Mater.* **2014**, *370*, 68.
[27] M. Schneider, H. Hoffmann, J. Zweck, *Appl. Phys. Lett.* **2001**, *79*, 3113.
[28] T. Kimura, Y. Otani, H. Masaki, T. Ishida, R. Antos, J. Shibata, *Appl. Phys. Lett.* **2007**, *90*, 132501.
[29] R. Hertel, S. Gliga, M. Fähnle, C. Schneider, *Phys. Rev. Lett.* **2007**, *98*, 117201.
[30] V. P. Kravchuk, Y. Gaididei, D. D. Sheka, *Phys. Rev. B* **2009**, *80*, 100405.
[31] M. Kammerer, M. Weigand, M. Curcic, M. Noske, M. Sproll, A. Vansteenkiste, B. Van Waeyenberge, H. Stoll, G. Woltersdorf, C. H. Back, Gisela Schuetz, *Nat. Commun.* **2011**, *2*, 279.
[32] E. Pinilla-Cienfuegos, S. Mañas-Valero, A. Forment-Aliaga, E. Coronado, *ACS Nano* **2016**, *10*, 1764.
[33] K. Yamada, S. Kasai, Y. Nakatani, K. Kobayashi, H. Kohno, A. Thiaville, T. Ono, *Nat. Mater.* **2007**, *6*, 270.
[34] D. Yu, J. Kang, J. Berakdar, C. Jia, *NPG Asia Mater.* **2020**, *12*, 36.
[35] J. Ding, G. N. Kakazei, X. Liu, K. Y. Guslienko, A. O. Adeyeye, *Sci. Rep.* **2014**, *4*, 4796.
[36] H. Cui, L. Cai, X. Yang, S. Wang, M. Zhang, C. Li, C. Feng, *Appl. Phys. Lett.* **2018**, *112*, 092404.
[37] Y. Gaididei, D. D. Sheka, F. G. Mertens, *Appl. Phys. Lett.* **2008**, *92*, 012503.
[38] R. Zhu, *arXiv preprint arXiv:1501.07293* **2015**.
[39] D. Jiles, *Introduction to Magnetism and Magnetic Materials*, CRC Press, Boca Raton, FL **2015**.
[40] Y. Tserkovnyak, A. Brataas, G. E. W. Bauer, *Phys. Rev. Lett.* **2002**, *88*, 117601.
[41] L. Yin, D. Wei, N. Lei, L. Zhou, C. Tian, G. Dong, X. Jin, L. Guo, Q. Jia, R. Wu, *Phys. Rev. Lett.* **2006**, *97*, 067203.
[42] R. C. O'handley, *Modern Magnetic Materials: Principles and Applications*, Wiley, New York **2000**.
[43] R. P. Boardman, Computer simulation studies of magnetic nanostructures, PhD thesis, University of Southampton **2005**.
[44] A. S. Moskalenko, Z. G. Zhu, J. Berakdar, *Phys. Rep.* **2017**, *672*, 1.